4D-LSM

Introduction

A comparative study of nine commonly used numerical methods was performed for predicting rock failure through international cooperation organized by the Discontinuous Deformation Analysis (DDA) commission of the International Society for Rock Mechanics (ISRM). Two steps of numerical modelling were conducted including a calibration procedure from given experimental results and a numerical prediction for benchmark tests with these calibrated parameters for three types of rocks. Through the comparison between different numerical and experimental results, the inherent weaknesses and strengths of different numerical methods in terms of predicting rock failure were identified and analysed.

1. Numerical simulations of experimental tests

1.1 UCS tests

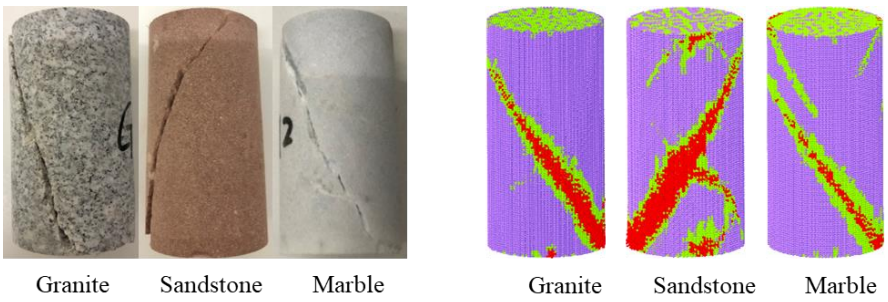

Fig. 1. Failure modes of rock samples after UCS tests in (a) laboratory tests; (b)4D-LSM.

Table 1 Input parameters of UCS test models

Experimental tests	Rock types	E （GPa）	μ	ρ (g/cm^3)	u_n	$dRatio$	c （MPa）	φ （° ）
UCS tests	Granite	42.25	0.27	2.63	0.05	0.1	29	52.18
	Sandstone	21.09	0.23	2.43	0.05	0.1	19	53.74
	Marble	59.69	0.23	2.85	0.05	0.1	22	51.11

1.2 BTS tests

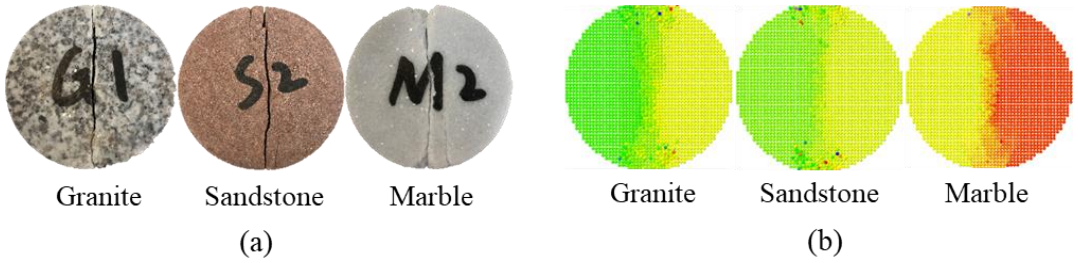

Fig. 2. Failure modes of rock samples after BTS tests in (a) laboratory tests; (b)4D-LSM.

Table 2 Input parameters of BTS test models

Experimental tests	Rock types	E （GPa）	μ	ρ (g/cm^3)	u_n	*dRatio*	c （MPa）	φ （°）
BTS tests	Granite	42.25	0.27	2.63	0.05	0.1	29	52.18
	Sandstone	21.09	0.23	2.43	0.05	0.1	19	53.74
	Marble	59.69	0.23	2.85	0.05	0.1	22	51.11

1.3 Benchmark tests

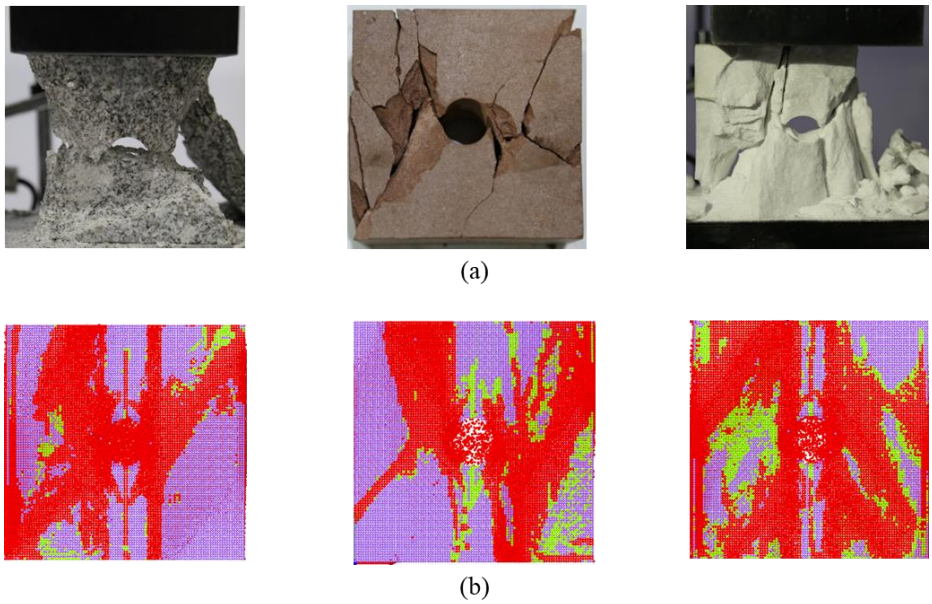

Fig. 3. Failure modes of rock samples after benchmark tests in (a) laboratory tests; (b)4D-LSM.

Table 3 Input parameters of benchmark test models

Experimental tests	Rock types	E （GPa）	μ	ρ (g/cm^3)	u_n	*dRatio*	c （MPa）	φ （°）
Benchmark tests	Granite	42.25	0.27	2.63	0.05	0.1	29	52.18
	Sandstone	21.09	0.23	2.43	0.05	0.1	19	53.74
	Marble	59.69	0.23	2.85	0.05	0.1	22	51.11

2. Discussion

2.1 Influence of end constraint

In uniaxial compression tests, the end constraint is a critical factor that affects the failure modes of rock samples due to the elastic mismatch between rocks and steel plates. As shown in Fig. 4a and 4b, although the whole samples are subjected to uniform uniaxial stress and displacement fields produced throughout the specimen, the specimen is restrained near its ends and prevented from deforming uniformly, and shear stress is produced at the specimen–steel platen contact. Therefore, stresses within the rock samples are not always uniaxial. To investigate the effects of the end constraint on the failure modes of rock samples, the bottom surface of the numerical models is fixed in y- and all directions to implement the uniform and radial restraint deformation of hollow rock plates, respectively (see Fig. 4c and 4d). The model parameters of rocks refer to the mechanical parameters of granite in Table 1. The particle size and the loading velocity for the two models are taken as 1 mm and 10 mm/s, respectively, and the other settings are consistent.

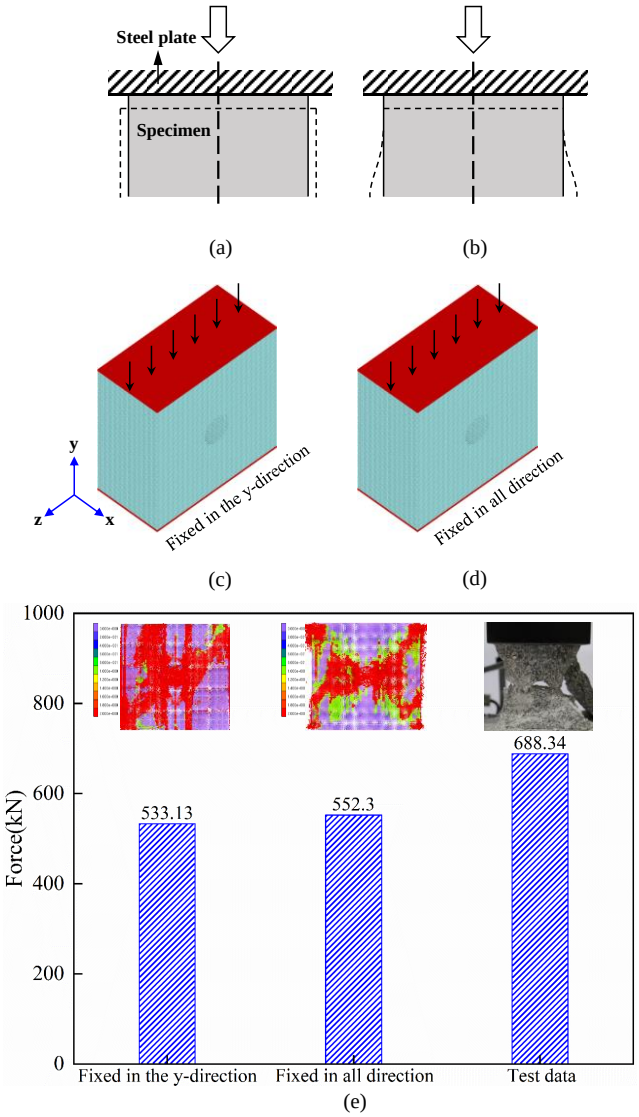

Fig. 4. Influence of the end constraint: (a) uniform deformation of the rock specimen; (b) deformation with complete radial restraint (after Brady and Brown[67]); (c) computational model fixed in the y-direction of the loading end; (d) computational model with loading condition fixed in all directions; and (e) numerical and experimental results.

Table 4 Input parameters of numerical models

Numerical model	E （GPa）	μ	ρ (g/cm^3)	u_n	*dRatio*	c （MPa）	φ （°）
Fixed in the y-direction	42.25	0.27	2.63	0.05	0.1	29	52.18
Fixed in all directions	42.25	0.27	2.63	0.05	0.1	29	52.18

2.2. Influence of the interface friction

To investigate the influence of the interface friction on numerical predictions, discontinuum-based spring bonds are incorporated into the 4D-LSM to simulate the discontinuous contact between the steel plate and rock sample. According to the work of Zhao,[68] the friction angle is adopted to represent the degree of interface friction (see Fig. 5a and 5b), and five computational models are set up with different friction angles θ (0°, 20°, 40°, 60°, and 80°). For the material parameters of the steel plates, the elastic modulus is 213 GPa, the Poisson's ratio is 0.25, and the density of 7780 kg/m^3. The joint normal and shear stiffness are both taken as 5 GPa/mm. Other settings are consistent with the above simulation utilized in Section 1.1.

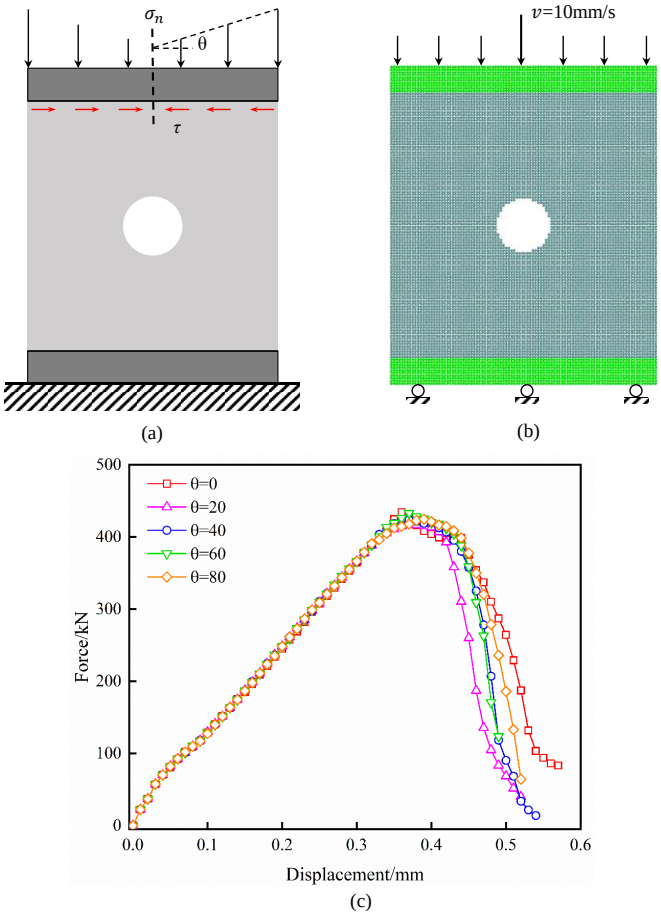

Fig. 5. Influence of the interface friction between the loading platen and specimen: (a) schematic of the friction angle; (b) computational model setup and boundary conditions; and (c) numerical results.

Table 5 Input parameters of numerical models

Numerical model	E （GPa）	μ	ρ (g/cm^3)	u_n	*dRatio*	c （MPa）	φ （°）
Benchmark test	42.25	0.27	2.63	0.05	0.1	29	52.18

2.3. Influence of the strength parameters

In the sections above, the peak strength of rocks predicted by 4D-LSM still underestimated the measured values, which is common in most numerical methods. It is necessary to investigate the effect of strength parameters on numerical predictions. Here, two main parameters of rocks (uniaxial tensile strength (UTS) and cohesion) were selected for sensitivity analysis, and internal frictional angles were chosen as default values. Moreover, we considered the effect of the UCS/T ratio, and the UTS (σ_t) of rocks can be calculated from cohesion based on the Mohr-Coulomb criterion as follows:

$$\sigma_t = \frac{2\cos\varphi}{R(1-\sin\varphi)}c \tag{2}$$

where c is the cohesion, φ is the internal friction angle, and R is the UCS/UTS ratio, respectively. Then, numerical simulations were conducted based on different cohesions and corresponding calculated UTSs for every type of rock.

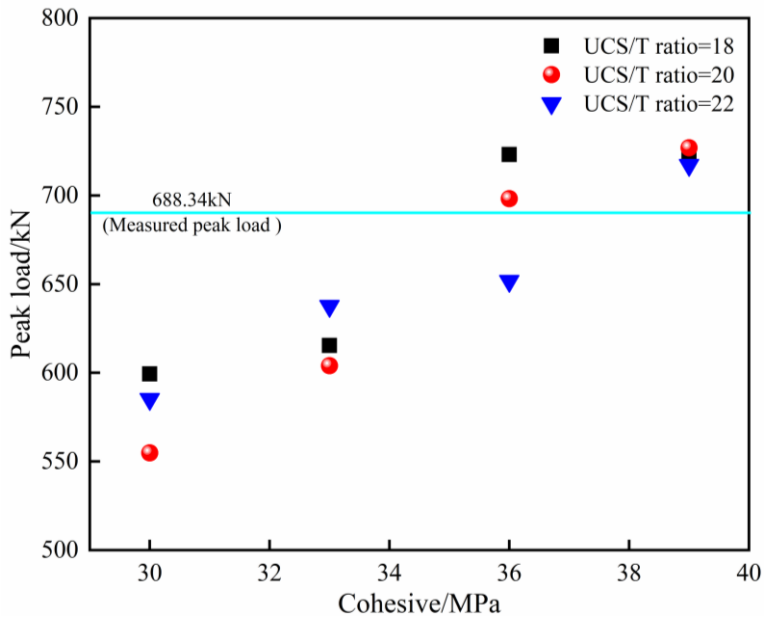

Fig. 6. Influence of different UCS/T ratios of granite on numerical predictions.

2.4. Influence of rock heterogeneity

The influence of material heterogeneity on the numerical simulation is considered based on the adjusted parameters model for granite in Section 5.3. The random two-phase models were employed to implement material heterogeneity, where material properties were randomly assigned to different particles for hollow plate models. The heterogeneity ratio H is defined as the proportion of the enriched particles to total particles. The larger the heterogeneity ratio H is, the greater heterogeneity the numerical model has. As shown in Fig. 7a, four computational models are set up with different values of heterogeneity ratio H (0.0, 0.1, 0.3, 0.5), and other settings are consistent with the above simulation utilized in Section 2.3.

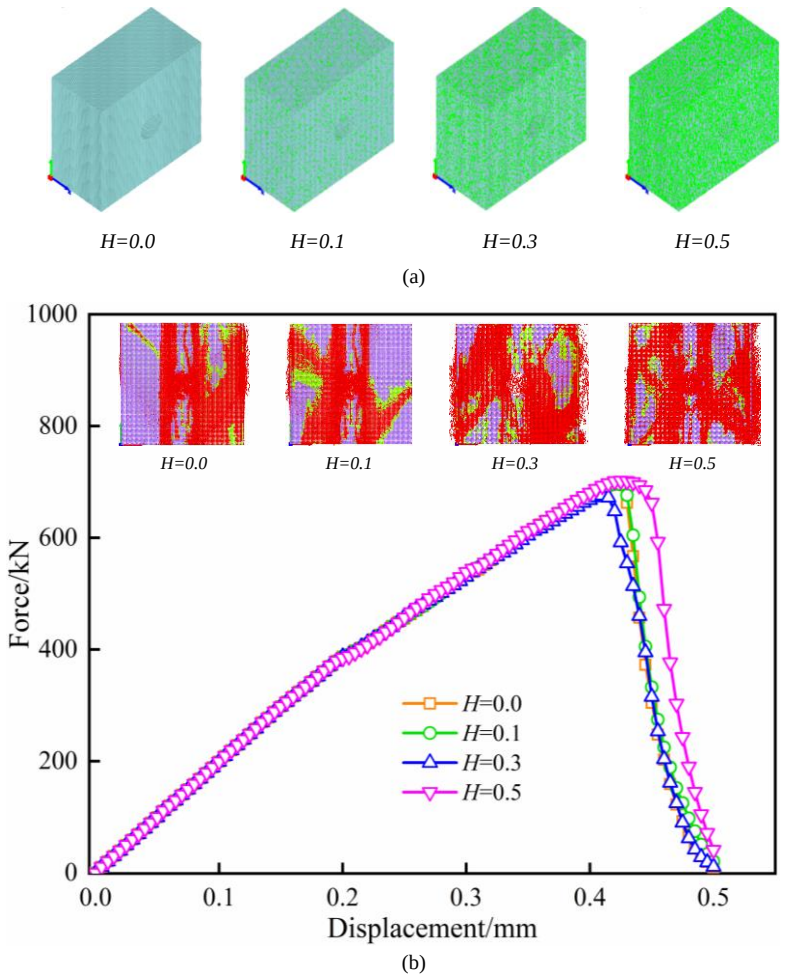

Fig. 7. Influence of material heterogeneity: (a) computational models with different heterogeneity ratios; (b) numerical results.

Table 6 Input parameters of numerical models

Numerical model	E （GPa）	μ	ρ (g/cm^3)	u_n	$dRatio$	c （MPa）	φ （°）
Material 1	42.25	0.27	2.63	0.05	0.1	29	52.18
Material 2	42.25	0.27	2.63	0.05	0.1	2900	52.18

2.5. Influence of different particle packing

In the previous section, the particle model in 4D-LSM is placed in a regular arrangement, and the computational domain is divided into a series of the same cubic, which may involve some error presentation of curved surfaces geometries, and

ultimately affect the numerical prediction. In this section, the irregular particle models for calibration and benchmark tests are generated based on an open-source meshing code, DISTMESH,[69] which can create an adaptive triangular mesh along the smoothed curved boundary. As shown in Fig. 12a, the irregularity along the curved boundary in a regular arrangement can be eliminated through the irregular particle model. Two steps of numerical simulation were conducted for the irregular particle model for three types of rocks with the same boundary conditions and parameters as the regular particle model in Section 2.3.

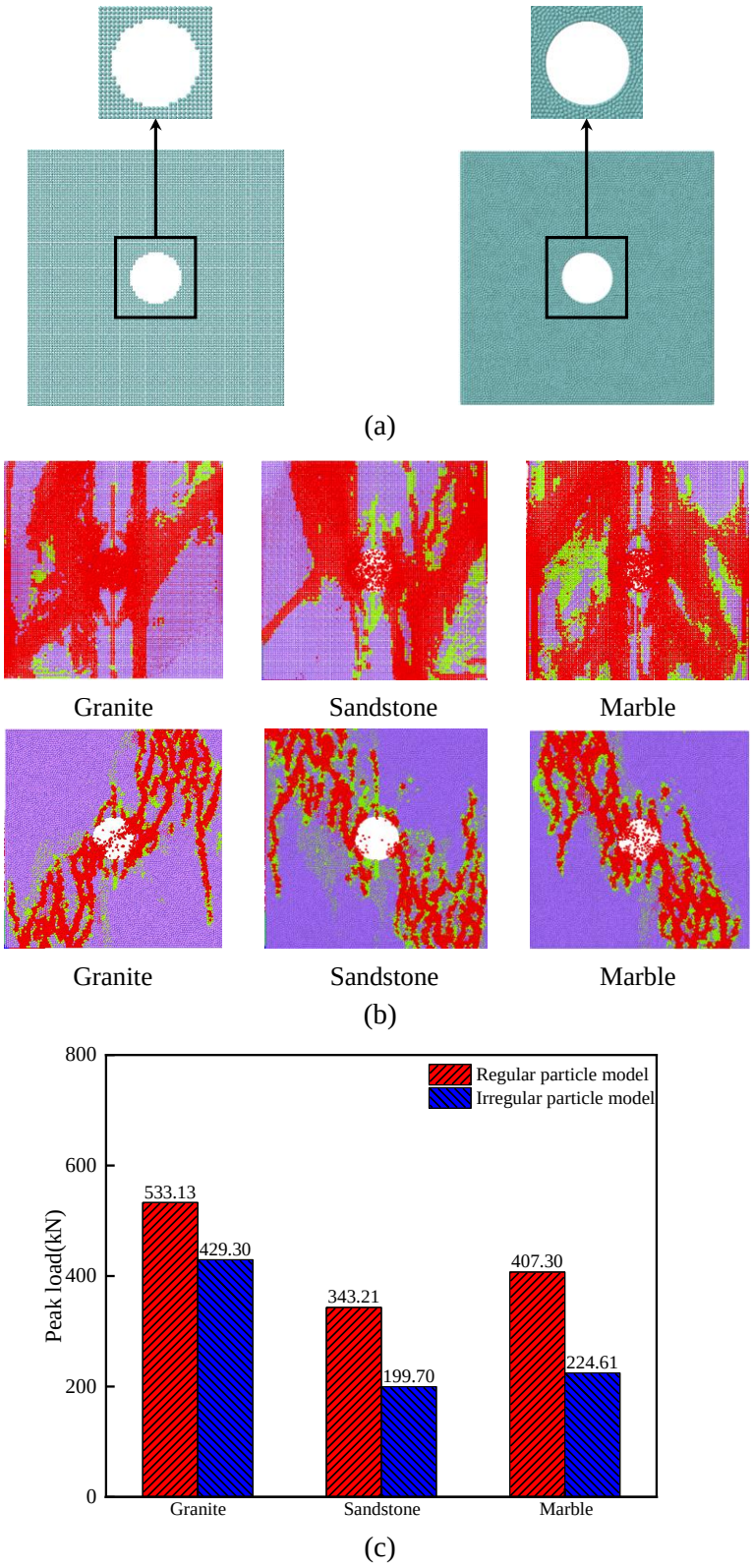

Fig. 12. (a) The hollow plate model with regular particle and irregular particle arrangement; (b) the failure modes of different particle models for three types of rocks; (c) numerical predictions for different particle models.

Table 7 Input parameters of numerical models

Numerical model	E （GPa）	μ	ρ (g/cm^3)	u_n	$dRatio$	c （MPa）	φ （°）
Regular particle model	42.25	0.27	2.63	0.05	0.1	29	52.18
Irregular particle model	42.25	0.27	2.63	0.05	0.1	29	52.18

2.6. Influence of different rock failure criteria

In this section, the Hoek–Brown criterion was incorporated into 4D-LSM to perform two steps of numerical simulation for three types of rocks and compared the numerical results with the Mohr-Coulomb criterion in 4D-LSM, which has been presented in the previous section. The Hoek–Brown criterion adopted to predict the strength of the intact rock at failure is expressed as follows:[70, 71]

$$\sigma_1 = \sigma_3 + \sigma_{c,i}\left(m_i \frac{\sigma_3}{\sigma_{c,i}} + 1\right)^{0.5} \tag{3}$$

where, m_i is the material constant for the intact rock, $\sigma_{c,i}$ is the UCS of intact rock, and σ_3 and σ_1 are the minor and major effective principal stresses at failure, respectively. The UCS of intact rock can be obtained by setting σ_3=0 in Eq. (3):

$$\sigma_c = \sigma_{c,i} \tag{4}$$

Moreover, Hoek and Brown[72] suggested a tension cut-off for determining the uniaxial tensile strength of intact rock:

$$\sigma_t = \frac{-\sigma_{c,i}}{0.81m_i + 7} \tag{5}$$

Therefore, m_i values can be obtained by the following equation:

$$m_i = (R - 7)/0.81 \tag{6}$$

Then, the default values of m_i can be obtained from Eq. (6) as 18.72, 16.09, and 16.22 for granite, marble, and sandstone, respectively. The two steps of numerical simulations were conducted based on different m_i values for every type of rock.

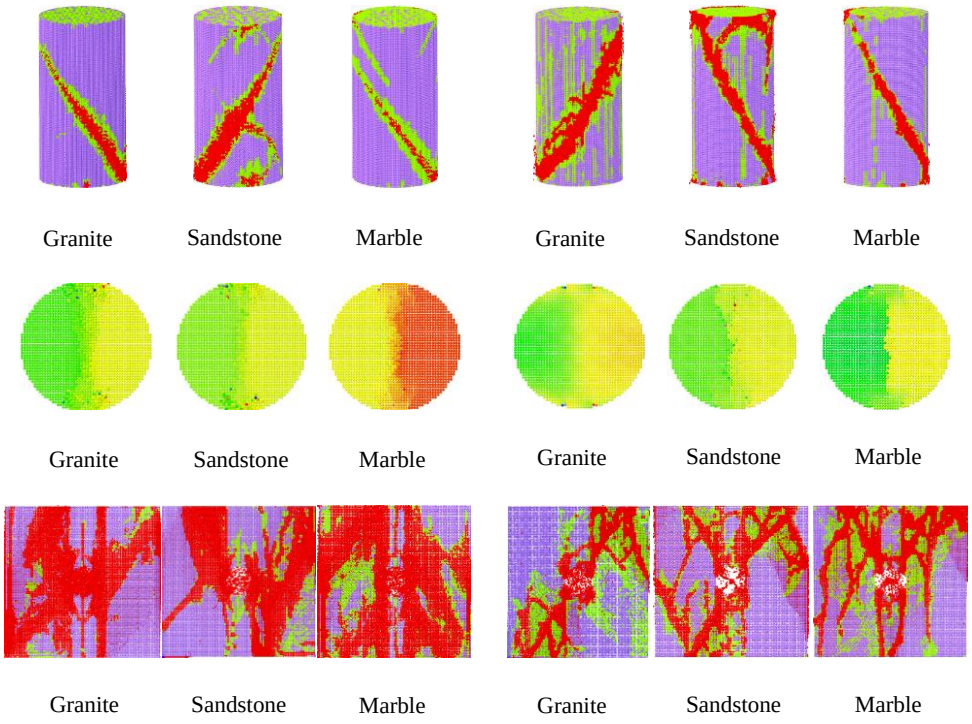

Fig. 13. Numerical simulations of calibration and benchmark tests from (a) the Mohr-Coulomb criterion and (b) the Hoek–Brown criterion.

Table 8 Input parameters of numerical models

Numerical model	Rock types	E （GPa）	μ	ρ (g/cm^3)	*dRatio*	m	s	a
H-B criterion model	Granite	42.25	0.27	2.63	0.2	22.16	1	0.5
	Sandstone	21.09	0.23	2.43	0.1	20	1	0.5
	Marble	59.69	0.23	2.85	0.15	20	1	0.5